# Pb–Graphene–Pb Josephson Junctions: Characterization in Magnetic Field

I. V. Borzenets, U. C. Coskun, H. Mebrahtu, and G. Finkelstein

***Abstract*—We fabricate superconductor–graphene–superconductor Josephson junctions with superconducting regions made of lead (Pb). The critical current through graphene may be modulated by the external magnetic field; the resulting Fraunhofer interference pattern shows several periods of oscillations, suggesting that the junction is uniform. Deviations from the perfect Fraunhofer pattern are observed, and their cause is explained by a simulation that takes into account the sample design.**

***Index Terms*—Josephson junctions, superconducting device measurements, superconducting films, superconducting materials, superconductor–normal–superconductor devices.**

## I. Introduction

THE PROPERTIES of superconductor–graphene–superconductor (SGS) junctions have attracted significant attention [1]–[5]. Unlike the conventional superconductor–normal-metal–superconductor (SNS) junctions, devices made with graphene allow for high tunability with the gate voltage. We have recently reported on SGS junctions, which use lead (Pb) as the superconducting material [5]. Lead has a relatively high critical temperature of 7.2 K, as compared with 1.2 K in the case of the commonly used aluminum. Indeed, we have observed supercurrent through graphene at temperatures as high as 2 K. In this paper, we characterize the properties of these junctions by applying magnetic field.

## II. Sample and Measurement Design

We fabricate the superconducting contacts to graphene from a palladium/lead (Pd/Pb) bilayer. First, we deposit a 2-nm layer of palladium, which creates transparent contacts to graphene [6], [7]; a 100-nm layer of lead is deposited *in situ* on top. The lateral width of the contacts is typically 500 nm. In this paper, we present the results measured on a junction about 20 $\mu$m wide and 400 nm long. (Commonly, the length of the junction is defined as the distance between the superconducting contacts and the width as the distance of the normal metal along the superconducting contacts.) In order to create such a wide junction, the leads are bent in two places to fit on a moderately sized graphene flake [see Fig. 1(a)]. We show that this particular sample design has certain nontrivial consequences.

We measured the sample electronic properties using a pseudo four-probe setup [see Fig. 1(a)]. The junction is biased by current $I$, which contains a small ac component, and the ac voltage across the junction is measured using a lock-in amplifier. The carrier density in graphene can be tuned by the back-gate voltage $V_{\rm gate}$, but for the results presented, the gate voltage is set at zero. Finally, a perpendicular magnetic field can be applied using two methods. Conventionally, field $B_{\rm ext}$ can be created by an external solenoid magnet. Alternatively, we send current $I_L$ along one of the superconducting leads [see Fig. 1(a)], inducing a field that we label as $B_L$. The advantage of the second method is that the required small fields can be easily obtained and rapidly changed. In this sample, we have calibrated $B_L$ to be equal to 0.95 T/A $I_L$ (see details below).

## III. Results

The Pd/Pb electrodes become superconducting at a temperature of ≈7 K, and the SGS junctions begin to exhibit enhanced zero-bias conductance at temperatures of ≈5 K. Below ≈2 K, a fully formed supercurrent branch is clearly observed [5]. Fig. 1(c) demonstrates the differential conductance $R \equiv dV/dI$ versus the bias current $I$ (vertical axis) and the magnetic field $B_L$ (horizontal axis) measured at several temperatures. The dark areas of the maps in Fig. 1(c) correspond to the regions of suppressed resistance. The regions are bound by a critical current $I = I_C$, above which the junction becomes normal. The value of $I_C$ increases as the temperature is lowered and saturates around $I_C \approx 0.5$ $\mu$A at zero magnetic field [see the lowest map in Fig. 1(c)]. When $B_L$ is applied, $I_C$ oscillates in a way closely resembling the Fraunhoffer diffraction pattern [10]. Several oscillations of $I_C$ can be observed at the lowest temperature; this suggests that the junction is uniform.

We next apply an external magnetic field $B_{\rm ext}$, which is found to shift the modulation pattern of Fig. 1(c) in the horizontal direction (Fig. 2). The shift is linear in $B_{\rm ext}$; indeed, at the center of the pattern, the external field and the one induced by $I_L$ cancel each other. The observed rate of the shift allows

Manuscript received February 27, 2012; revised April 17, 2012 and May 1, 2012; accepted May 1, 2012. This paper was recommended by Associate Editor O. Mukhanov. The work was supported by the Division of Materials Sciences and Engineering, Office of Basic Energy Sciences, U.S. Department of Energy, under Award DE-SC0002765.

I. V. Borzenets was with Duke University, Durham, NC 27708 USA (e-mail: borzenets@gmail.com).

U. C. Coskun was with Duke University, Durham, NC 27708 USA. He is currently with the University of Illinois, Urbana-Champagne, Urbana, IL 61801 USA (e-mail: uccoskun@gmail.com).

H. Mebrahtu was with Duke University, Durham, NC 27708 USA. He is currently with the Intel Corporation, Santa Clara, CA 95054-1549 USA (e-mail: htm@phy.duke.edu).

G. Finkelstein is with Duke University, Durham, NC 27708 USA (e-mail: gleb@phy.duke.edu).

Color versions of one or more of the figures in this paper are available online at http://ieeexplore.ieee.org.

Digital Object Identifier 10.1109/TASC.2012.2198472

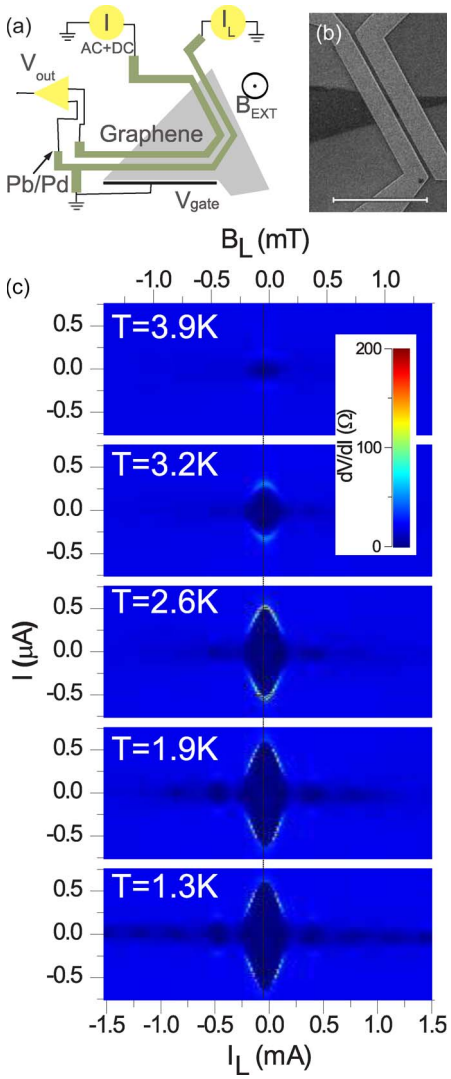


Fig. 1. (a) Schematic of the measurement setup. The metal leads form a "⊔" shape in order to increase their length. Bias current $I$ with a small ac modulation is sent through the junction. The resulting ac component of the voltage across the junction is measured using a lock-in amplifier allowing one to record the differential resistance $R \equiv dV/dI$. An external magnetic field $B_{\rm ext}$ is applied by a superconducting solenoid. In addition, a magnetic field $B_L$ is created by sending current $I_L$ along one of the leads of the junction. Sweeping current $I_L$ allows to apply a very small magnetic field $B_L$. (b) Scanning electron micrograph (SEM) of a graphene-based SNS Josephson junction similar but smaller than the one presented in this paper. (Junctions used for the measurement were not imaged in order to preserve the quality of graphene.) The dark triangular area is a single-layer graphene flake, and the metal contacts are made from lead (Pb) with a thin contact layer of palladium (Pd), which extends 10–20 nm past the Pb. The image was taken using an FEI XL30 SEM with a "ultrahigh resolution" TLD detector at the accelerating voltage of 1 kV. (c) Differential resistance $dV/dI$ maps measured versus bias current $I$ and magnetic-field-inducing current $I_L$. Regions of vanishing $R$ appear dark. Each panel corresponds to the measurement at a different temperature. Enhanced zero-bias conductance develops around ≈4 K for small fields $B_L$. With lower temperatures, more and more critical current modulations appear, and the Fraunhofer interference pattern is observed. At the base temperature of 1.3 K, the critical current is seen at fields beyond 5 mT (see Fig. 5). Observing many oscillations suggest that the junction is highly uniform.

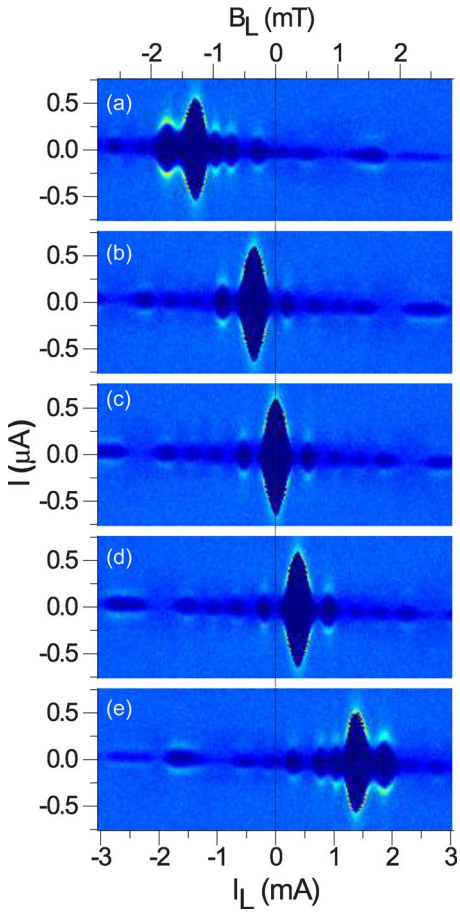


Fig. 2. $R(I, I_L)$ maps [like those in Fig. 1(c)] measured at different values of the external magnetic field (a) $B_{\rm ext} = -1.3$ mT, (b) $B_{\rm ext} = -0.36$ mT, (c) $B_{\rm ext} = 0$, (d) $B_{\rm ext} = 0.36$ mT, and (e) $B_{\rm ext} = 1.3$ mT. Application of $B_{\rm ext}$ shifts the modulation pattern, (b)–(d) so that at its center $B_{\rm ext}$ and $B_L$ cancel each other. Since the cancellation is not perfect, (a) the pattern gets distorted, compared with the pattern at the zero external field (c). Opposite orientation of the external magnetic field (e) results in mirror reversal of the distortions. $T = 1.3$ K.

us to fix conversion $B_L = 0.95$ T/A $I_L$ mentioned earlier. This factor is also consistent with our order-of-magnitude estimates. Furthermore, the shift of the pattern by $\Phi_0$ in an external magnetic field of 0.36 mT allows us to extract the effective area of 5.6 $\mu$m$^2$. While this area is smaller than 8 $\mu$m$^2$ expected from the designed sample dimensions of $W = 20$ $\mu$m by $L = 0.4$ $\mu$m, it is quite likely that length $L$ between the leads is reduced in the process of lithography or that the magnetic field is modified due to the presence of the superconducting leads.

When the magnetic field $B_{\rm ext}$ of the order of tens of millitesla is applied to the sample, the observed pattern becomes distorted even after the field is returned back to zero (see Fig. 3). It is clear that the resulting pattern at $B_{\rm ext} = 0$ [see Fig. 3(a)] is very different from the original one [see Fig. 2(c)]. We can partially recover the original pattern by setting $B_{\rm ext} \approx 3.4$ mT [see Fig. 3(b)]. When comparing the resulting pattern to the original one [see Fig. 2(c)], we notice that the critical current is slightly suppressed and the sidelobes have somewhat random heights. We attribute these distortions and the shift from the zero field to the trapping of magnetic flux in the superconducting film [11], [12]. Indeed, the undistorted pattern shown in Fig. 2(c) can be restored following the thermal cycling to ≈10 K, beyond the critical temperature of lead.

Interestingly, at fields less than those causing trapped flux of Fig. 3, distortions of a different nature are introduced to the pattern [see Fig. 2(a)]. The first difference is that, returning

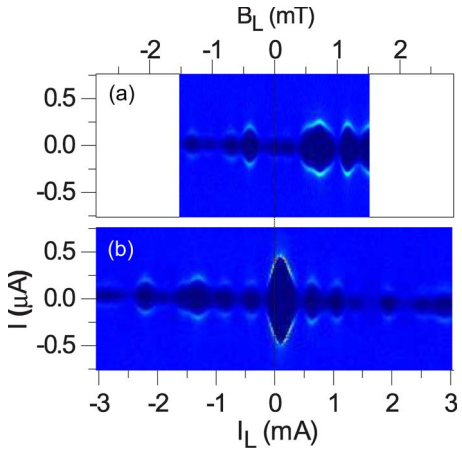


Fig. 3. $R(I, I_L)$ measurements taken after the perpendicular magnetic field was ramped beyond several tens of millitesla. (a) Measurement done when $B_{\rm ext}$ was returned back to zero. Clearly, the pattern is now vastly distorted. (b) Taken at $B_{\rm ext} = 3.4$ mT. At this field, the original critical current modulation pattern [see Fig. 2(c)] is partially restored. However, the central lobe shows a suppressed critical current, and the sidelobes form a distorted pattern. These permanent distortions are attributed to the trapped flux in the leads. Heating of the sample beyond the $T_C$ value of Pb is required in order to restore the symmetric patterns shown in Fig. 2(c).

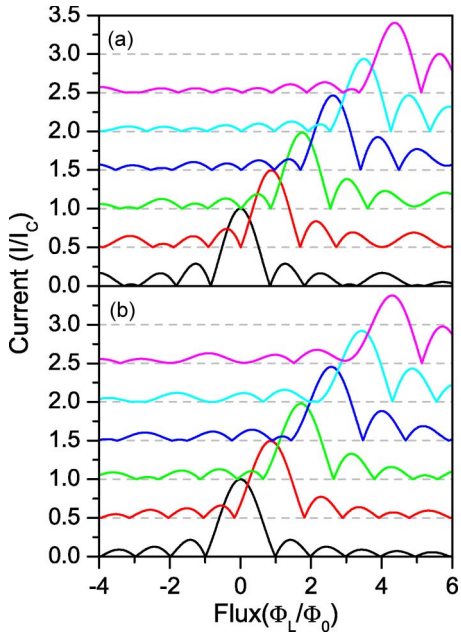


Fig. 4. Simulated critical current versus $I_L$ at several values of $B_{\rm ext}$. The bottom curve is taken at $B_{\rm ext} = 0$, and in each consecutive curve, the external flux $\Phi_{\rm ext}$ grows by the flux quantum $\Phi_0$. The phase difference between the two leads linearly grows along their length, proportionally to $I_L$; the horizontal axis is labeled in units of $\Phi_L$, i.e., the total flux induced by $I_L$. In addition, we assume discontinuous phase jumps positioned 2/5 and 3/5 along the length of the leads; this approximates the realistic shape of the sample, where the leads turn 90° around these two places (the major features appear insensitive to the exact locations of the discontinuities). (a) Case where the phase discontinuity is proportional to $I_L$. Specifically, we take each phase discontinuity equal to 0.1 $\Phi_L/\Phi_0$. (b) Case where the phase discontinuities are proportional to $B_{\rm ext}$ and equal to 0.1 $\Phi_{\rm ext}/\Phi_0$. Qualitatively, it is shown that, at zero $B_{\rm ext}$, panel A shows distortions of the interference pattern (similar to the ones shown in Fig. 5), whereas panel B displays a perfect Fraunhofer pattern (as expected, since the phase discontinuities are not induced). Another qualitative difference could be noticed at higher values of $B_{\rm ext}$, where the frequency of the oscillations to the left of the central peak (a) increases [consistent with the experimental results in Fig. 2(a) and (e)] and (b) decreases (inconsistent with the experiment).

to $B_{\rm ext} = 0$ restores the original pattern without any hysteresis. Second, the pattern demonstrates perfect symmetry under simultaneous reversal of both $B_{\rm ext}$ and $I_L$ [cf. Fig. 2(a) and (e)]. We associate this behavior with the fact that the phase difference is not linear along the length of the leads. Indeed, field $B_L$ may not be entirely uniform, so that it is not perfectly compensated by $B_{\rm ext}$. Most likely, the deviations of $B_L$ from uniformity are caused by the bends in the leads [schematic in Fig. 1(a)], at which points the phase difference experiences discontinuous steps proportional to $I_L$. The situation is very similar to the junctions with an artificial phase discontinuity controlled by an external current [13], [14]. Indeed, some of the features that we observe in Fig. 2(a) and (e), e.g., the strengthening of the sidelobe at the expense of the central lobe, resemble those found in [13] and [14].

## IV. Simulation

To describe the distortions found in Fig. 2(a) and (e), we consider a semirealistic model of the sample. We assume that the leads extend from $x = -W/2$ to $+W/2$; the position-dependent phase difference $\Phi_L(x)/\Phi_0$ induced by $B_L(x)$ is taken to be piecewise linear in $x$, with a slope proportional to $I_L$. Two identical discontinuous steps of $\Phi_L(x)$ are placed at $-W/10$ and $+W/10$. These points are close to the actual locations of the bends in the leads, but we checked that the main features of the simulation do not crucially depend on the details (i.e., the position of discontinuities or symmetry of their placement). We also include the effect of the external field, which induces flux $\Phi_{\rm ext}$. In our simulations, the current-phase relation is assumed to be sinusoidal. Although deviations from a sinusoidal relation have been recently observed in SGS junctions [15], the approximation should be adequate in our case, due to the relatively large distance between the leads ($L = 400$ nm) and the relatively high temperature of 1 K.

The simulated patterns of the critical current $I_C$ versus $I_L$ and $B_{\rm ext}$ are shown in Fig. 4. In the first simulation [see Fig. 4(a)], the strength of the phase discontinuities is taken to be proportional to $I_L$. Specifically, we take each phase discontinuity equal to $0.1\Phi_L/\Phi_0$. On the other hand, in the second simulation [see Fig. 4(b)], the strength of the discontinuities is taken to be proportional to $B_{\rm ext}$ and equal to 0.1 $\Phi_{\rm ext}/\Phi_0$. The main features observed in Fig. 2 are qualitatively reproduced in both simulations, such as the overall shift of the $I_C(I_L)$ pattern in $B_{\rm ext}$, the growing distortion of the $I_C(I_L)$ pattern in $B_{\rm ext}$, and the growing strength of the sidelobe on the high-current side of the pattern at the expense of the central lobe.

However, there are two key differences between the two simulation. First, at higher values of $B_{\rm ext}$, the frequency of the oscillations to the left of the central peak increases in simulation A [consistent with the experimental results in Fig. 2(a) and (e)] and decreases in simulation B (inconsistent with the experiment). Second, at $B_{\rm ext} = 0$, simulation B produces a perfect Fraunhofer pattern. (This is expected as no phase discontinuities are present at the zero external field in this case.) Simulation A, on the contrary, while producing a pattern similar to the perfect Fraunhofer pattern $I \propto \sin(\pi I_L/I_L^{(0)})/I_L$, shows

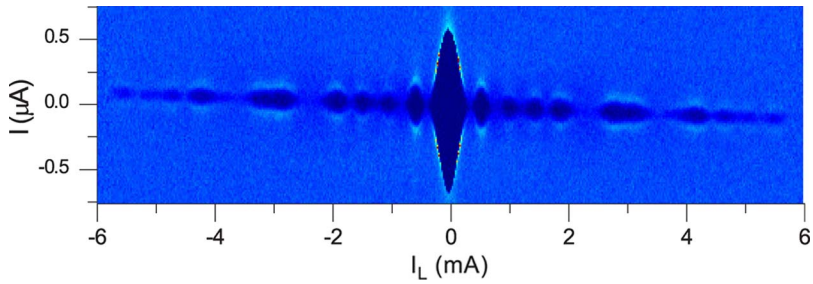


Fig. 5. Differential resistance $dV/dI$ map measured versus bias current $I$ and current $I_L$ inducing magnetic field. These data are similar to Fig. 2(c) but are extended up to $I_L = 6$ mA. Note the suppression of the selected sidelobes (see $I_L \approx \pm 2.5$ mA and $\pm 3.5$ mA). This suppression of sidelobes qualitatively resembles the simulation results (see Fig. 4; $B_{\rm ext} = 0$, $\Phi_L/\Phi_0 \approx \pm 3$ and $\pm 5$). The tilt of the pattern is an artifact of $I_L$ flowing through the normal part of the sample, thus creating a voltage drop that shifts the zero of $I$.

noticeable deviations. Namely, some of the sidelobes are almost suppressed to zero, whereas further lobes at higher $I_L$ regain strength. A similar behavior is indeed observed in the experiment (see Fig. 5). Note the region of the suppressed critical current at $I_L \approx \pm 2.3$ mA in Fig. 2(c), and its reappearance at higher $I_L \approx \pm 3.5$ mA. As such, we conclude that the phase discontinuities proportional to $I_L$ have to be included to explain the experimentally observed patterns.

## V. Conclusion

We have demonstrated the magnetic-field-induced quasi-periodic modulation of critical current in Pb–graphene–Pb structures, which suggests their spatial uniformity. The magnetic field can be applied by running a current through one of the superconducting leads within the same structure, resulting in a simple yet efficient method to *in situ* control the critical current. The dependence of the critical current on the thus applied magnetic field deviates from the perfect Fraunhofer interference pattern. The difference has been attributed to the presence of bends in the superconducting leads; a simple simulation supports this explanation.

## References

[1] H. B. Heersche, P. Jarillo-Herrero, J. B. Oostinga, L. M. K. Vandersypen, and A. F. Morpurgo, "Bipolar supercurrent in graphene," *Nature*, vol. 446, no. 7131, pp. 56–59, Mar. 2007.

[2] F. Miao, S. Wijeratne, Y. Zhang, U. C. Coskun, W. Bao, and C. N. Lau, "Phase-coherent transport in graphene quantum billiards," *Science*, vol. 317, no. 5844, pp. 1530–1533, Sep. 2007.

[3] X. Du, I. Skachko, and E. Y. Andrei, "Josephson current and multiple Andreev reflections in graphene SNS junctions," *Phys. Rev. B*, vol. 77, no. 18, p. 184 507, 2008.

[4] C. Ojeda-Aristizabal, M. Ferrier, S. Gueron, and H. Bouchiat, "Tuning the proximity effect in a superconductor–graphene–superconductor junction," *Phys. Rev. B*, vol. 79, no. 16, pp. 165 436-1–165 436-5, 2009.

[5] I. V. Borzenets, U. C. Coskun, S. J. Jones, and G. Finkelstein, "Phase diffusion in graphene-based Josephson junctions," *Phys. Rev. Lett.*, vol. 107, no. 13, pp. 137 005-1–137 005-4, Sep. 2011.

[6] B. Huard, N. Stander, J. A. Sulpizio, and D. Goldhaber-Gordon, "Evidence of the role of contacts on the observed electron-hole asymmetry in graphene," *Phys. Rev. B*, vol. 78, no. 12, pp. 121 402-1–121 402-4, 2008.

[7] F. Xia, V. Perebeinos, Y. Lin, Y. Wu, and P. Avouris, "The origins and limits of metal–graphene junction resistance," *Nature Nano.*, vol. 6, no. 3, pp. 179–184, Feb. 2011.

[8] K. S. Novoselov, D. Jiang, F. Schedin, T. J. Booth, V. V. Khotkevich, S. V. Morozov, and A. K. Geim, "Two-dimensional atomic crystals," in *Proc. Nat. Acad. Sci.*, Jul. 2005, vol. 102, no. 30, pp. 10 451–10 453.

[9] A. C. Ferrari, J. C. Meyer, V. Scardaci, C. Casiraghi, M. Lazzeri, F. Mauri, S. Piscanec, D. Jiang, K. S. Novoselov, S. Roth, and A. K. Geim, "Raman spectrum of graphene and graphene layers," *Phys. Rev. Lett.*, vol. 97, no. 18, pp. 187 401-1–187 401-4, Oct. 2006.

[10] M. Tinkham, *Introduction to Superconductivity*. New York: McGraw-Hill, 1996.

[11] S. L. Miller, K. R. Biagi, J. R. Clem, and D. K. Finnemore, "Critical currents of cross-type superconducting–normal–superconducting junctions in perpendicular magnetic fields," *Phys. Rev. B*, vol. 31, no. 5, pp. 2684–2693, 1985.

[12] V. N. Gubankov, M. P. Lisitskii, I. L. Serpuchenko, and M. V. Fistul, "Effect of Abrikosov vortices on the critical current of a Josephson junction," *Sov. Phys. JETP*, vol. 73, p. 734, 1991.

[13] T. Gaber, E. Goldobin, A. Sterck, R. Kleiner, D. Koelle, M. Siegel, and M. Neuhaus, "Nonideal artificial phase discontinuity in long Josephson $0 - \kappa$ junctions," *Phys. Rev. B*, vol. 72, p. 054522, 2005.

[14] E. Goldobin, A. Sterck, T. Gaber, D. Koelle, and R. Kleiner, "Dynamics of semifluxons in Nb long Josephson $0 - \pi$ junctions," *Phys. Rev. Lett.*, vol. 92, no. 5, p. 057005, 2003.

[15] C. Chialvo, I. C. Moraru, D. J. Van Harlingen, and N. Mason, Current-Phase Relation of Graphene Josephson Junctions, 2010, arXiv:1005.2630v2.

**I. V. Borzenets**, biography not available at the time of publication.

**U. C. Coskun**, biography not available at the time of publication.

**H. Mebrahtu**, biography not available at the time of publication.

**G. Finkelstein**, biography not available at the time of publication.